

THE SUBMILLIMETER PROPERTIES OF EXTREMELY RED OBJECTS

E. H. WEHNER,¹ A. J. BARGER,^{1,2,3} J.-P. KNEIB⁴

Accepted by the Astrophysical Journal Letters

ABSTRACT

We use deep near-infrared and submillimeter observations of three massive lensing cluster fields, A370, A851, and A2390, to determine the average submillimeter properties of a K' -selected sample. The 38 Extremely Red Objects (EROs; $I - K' > 4$) with $K' < 21.25$ have a very significant error-weighted mean $850 \mu\text{m}$ flux of $1.58 \pm 0.13 \text{ mJy}$. The ERO contribution to the $850 \mu\text{m}$ background is $1.88 \pm 0.16 \times 10^4 \text{ mJy deg}^{-2}$, or about half the background light. The 17 Very Red Objects (VROs; $3.5 < I - K' < 4$) are also significantly detected ($1.32 \pm 0.19 \text{ mJy}$), bringing the combined VRO and ERO contribution to $2.59 \pm 0.19 \times 10^4 \text{ mJy deg}^{-2}$. There is a substantial systematic uncertainty (about a factor of two) in this value due to field-to-field variation, but even with this uncertainty it is clear that a large fraction of the $850 \mu\text{m}$ background arises from red objects. An analysis of the VRO and ERO number counts shows that half of the population's $850 \mu\text{m}$ light arises in objects with demagnified magnitudes $K' < 20$ and half in fainter objects. On the basis of the $I - J$ versus $J - K'$ colors of the galaxies, the bulk of the submillimeter signal appears to arise from the dusty starburst galaxies in the red object population rather than from the high-redshift elliptical galaxies.

Subject headings: cosmology: observations — galaxies: evolution — galaxies: formation

1. INTRODUCTION

Extremely Red Objects (EROs) have been the subject of many studies since their discovery (e.g., Cowie et al. 1990; Hu & Ridgway 1994). Two scenarios can explain the unusually red colors of the EROs: old stellar populations at $z > 1$ (e.g., Dunlop et al. 1996; Spinrad et al. 1997; Soifer et al. 1999; Cimatti et al. 2002) or dust-enshrouded galaxies (e.g., Graham & Dey 1996; Cimatti et al. 1998; Smith et al. 2001). The starlight from dusty galaxies is reprocessed and reemitted in the rest wavelength far-infrared band. For high redshift sources, this light is redshifted into the submillimeter. Recently, a number of possible ERO counterparts to submillimeter detected sources have been discovered (e.g., Smail et al. 1999, 2002; Barger, Cowie, & Richards 2000; Ivison et al. 2002).

The *COBE* satellite found that the submillimeter extragalactic background light (EBL) has approximately the same integrated energy density as the optical EBL (Puget et al. 1996; Fixsen et al. 1998); thus, a large fraction of starlight is reradiated by dust. To determine the high-redshift star formation, the sources that comprise the submillimeter EBL need to be determined. Here we use deep submillimeter and near-infrared (NIR) imaging of three massive lensing cluster fields to determine the submillimeter properties of the ERO population. Two advantages of observing cluster fields are that background sources are magnified and mean source separations on the sky are increased.

In § 2 we briefly describe our I , J , K' , and $850 \mu\text{m}$ data. The $15''$ beam size of SCUBA (Holland et al. 1999)

on the 15 m James Clerk Maxwell Telescope⁵ prohibits us from making individual matches between submillimeter and optical/NIR sources. However, in § 3 we analyze our data statistically and find that EROs, as a class, have a significant submillimeter flux and produce much of the $850 \mu\text{m}$ EBL. In § 4 we use our NIR photometry and lensing corrections to calculate the ERO surface densities to $K' = 24$. We analyze where in K' magnitude the $850 \mu\text{m}$ flux arises. Using the I , J , K' colors, we differentiate between evolved galaxies and dust-reddened starbursts to show that the $850 \mu\text{m}$ light primarily arises in the latter class of object.

2. DATA AND SAMPLE SELECTION

We constructed K' catalogs for our three cluster fields using data obtained with the Cooled Infrared Spectrograph and Camera for OHS (CISCO; Motohara et al. 1998) on the Subaru⁶ 8.2 m telescope. The detector is a 1024×1024 HgCdTe HAWAII array with a $0.111''$ pixel scale and an $\sim 2' \times 2'$ field-of-view. The K' exposures are 15.4 ks (A370), 3.84 ks (A851), and 15.4 ks (A2390). J -band data were also obtained with the same instrument. Details of the observations and data reduction can be found in Cowie et al. (2001; A370 and A2390) and L. L. Cowie et al., in preparation (A851). The image quality of the K' images is $0.66''$ FWHM. We used K' magnitudes measured in $2''$ diameter apertures to determine colors, and we used isophotal magnitudes to 2% of the peak surface brightness for total magnitudes. We es-

¹Department of Astronomy, University of Wisconsin-Madison, 475 North Charter Street, Madison, WI 53706

²Department of Physics and Astronomy, University of Hawaii, 2505 Correa Road, Honolulu, HI 96822

³Institute for Astronomy, University of Hawaii, 2680 Woodlawn Drive, Honolulu, Hawaii 96822

⁴Observatoire Midi-Pyrénées, 14 Avenue E. Belin, 31400, Toulouse, France

⁵The James Clerk Maxwell Telescope is operated by the Joint Astronomy Centre on behalf of the UK Particle Physics and Astronomy Research Council, the Netherlands Organization for Scientific Research, and the Canadian National Research Council

⁶The Subaru telescope is operated by the National Astronomical Observatory of Japan.

timated the noise in the images by measuring aperture magnitudes at a number of blank sky positions. The 5σ limit for the shallowest of the fields is $K' = 21.25$; we adopt this limit for the entire K' sample selection.

We measured $2''$ diameter aperture I -band magnitudes for the K' samples from images obtained with either the Low-Resolution Imaging Spectrometer (LRIS; Oke et al. 1995) or the Echellette Spectrograph and Imager (ESI; Epps & Miller 1998) on the Keck⁷ 10 m telescopes. The data are described in Cowie et al. (2001; A370 and A2390) and Smail et al. (1999; A851). The 2σ limit for the shallowest of the fields is $I = 26$; we adopt this limit for the entire sample.

Finally, we measured $850\ \mu\text{m}$ fluxes at the K' source positions from ultradeep SCUBA jiggle maps. We used beam-weighted extraction routines that include both the positive and negative portions of the beam profile. The total exposure times are 133.1 ks (A370), 59.3 ks (A851), and 78.1 ks (A2390). The 1σ sensitivities, including both fainter sources and correlated noise, are 0.45 mJy (A370), 0.87 mJy (A851), and 0.71 mJy (A2390). The data are described in Cowie, Barger, & Kneib (2002).

3. SUBMILLIMETER PROPERTIES OF EROS AND THEIR CONTRIBUTION TO THE SUBMILLIMETER EBL

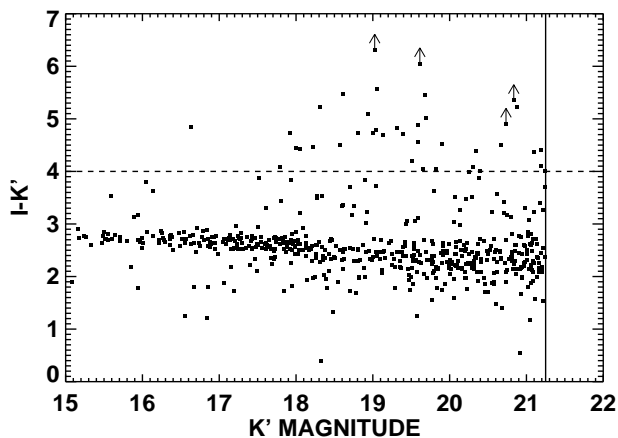


FIG. 1.— $I - K'$ versus K' for the combined K' samples in the A370, A851, and A2390 fields. The vertical line denotes the $K' = 21.25$ (5σ) limit adopted. The upward pointing arrows denote sources that were not detected above $I = 26$ (2σ).

Figure 1 shows the $I - K'$ versus K' color-magnitude diagram. Most of the sources are cluster members. The cluster color-magnitude relationship is clearly visible and matches the measured relations for clusters at these redshifts (e.g., Kodama et al. 1998). Thirty-eight galaxies have $I - K' > 4$, classifying them as EROs, and fifty-five have $I - K' > 3.5$. We classify galaxies with $3.5 < I - K' < 4$ as Very Red Objects (VROs). The $11.5\ \text{arcmin}^2$ area covered by the K' data is somewhat smaller than the $18.9\ \text{arcmin}^2$ area covered by the submillimeter data. A disproportionate number of the EROs and VROs lie in the A2390 cluster field (26 of the 38 sources with $I - K' > 4$, and 32 of the 55 sources with $I - K' > 3.5$). The excess may be associated with a very

high-redshift, evolved cluster lying behind A2390, as we discuss in § 4.

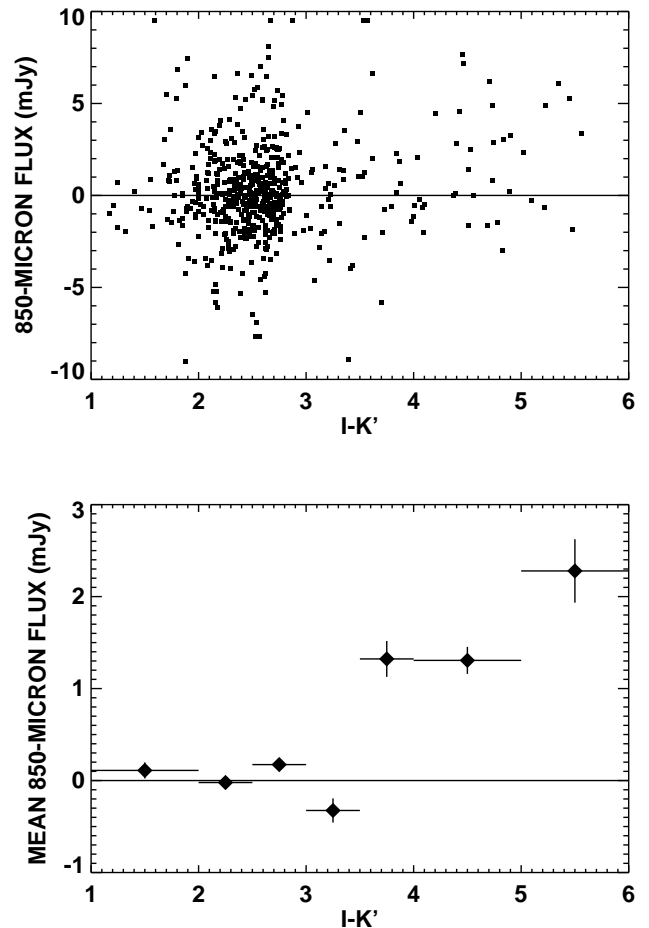


FIG. 2.— (a) $850\ \mu\text{m}$ flux and (b) error-weighted mean $850\ \mu\text{m}$ flux versus $I - K'$ color for the combined K' samples in the A370, A851, and A2390 fields. In (a) any sources with $850\ \mu\text{m}$ flux greater than $9.5\ \text{mJy}$ are plotted at $9.5\ \text{mJy}$. In (b) the vertical bars show the 1σ uncertainties and the horizontal bars show the color range sampled in each bin.

The $15''$ SCUBA beam size means that we cannot be certain which K' -selected galaxy is the true counterpart to a submillimeter source. However, by determining the error-weighted mean $850\ \mu\text{m}$ flux of the K' sources, we can make statistically significant statements regarding the relationship between submillimeter flux and source color. This is analogous to what Peacock et al. (2000) did for optical starbursts.

In Fig. 2a we plot submillimeter flux versus $I - K'$ color, and in Fig. 2b we plot error-weighted mean $850\ \mu\text{m}$ flux per color bin. Because submillimeter sources are not removed from the jiggle maps, the complex beam profile produced by the nod and chop observing pattern (there are twice as many negative as positive response points, but at half the sensitivity) means that the submillimeter flux distribution is non-Gaussian with an extended negative tail. A negative submillimeter flux will be measured for a K' -selected source positioned in the negative portion of the beam profile corresponding to a submillimeter source. Thus, there

⁷The W. M. Keck Observatory is operated as a scientific partnership among the California Institute of Technology, the University of California, and NASA, and was made possible by the generous financial support of the W. M. Keck Foundation.

are more high negative flux measurements in Fig. 2a than would be expected based on a simple Gaussian model with the quoted errors. The average signal of a set of random sources should, however, be zero, and the significance of the result can be determined from sets of Monte Carlo simulations of the same number of points randomly distributed in the fields (more details can be found in Cowie et al. 2002).

At low values of $I - K'$ the error-weighted mean $850 \mu\text{m}$ fluxes are consistent with zero; however, as $I - K'$ increases, there is a corresponding increase in the means (see Fig. 2b). The $I - K' > 4$ galaxies have an error-weighted mean of 1.58 ± 0.13 mJy. The formal error is based on the assumption of Gaussian statistics and may underestimate the true error, but the result is highly significant: 10000 Monte Carlo simulations yielded only one case where the same number of randomly positioned objects had a value equal or above the observed value. We tested whether the signal is arising from a small number of objects by eliminating the positive and negative tails: if the two (five) most positive and two (five) most negative sources are removed from the $I - K' > 4$ sample, the signal becomes 1.40 ± 0.14 mJy (1.48 ± 0.15 mJy). The $I - K' > 4$ objects in the A2390 field have a value of 1.41 ± 0.18 mJy, while those in the A370 and A851 fields have a value of 1.80 ± 0.20 mJy, so the mean submillimeter flux per ERO is consistent, even if we break down the sample. The $3.5 < I - K' < 4$ galaxies have an error-weighted mean of 1.32 ± 0.19 mJy; here 10000 simulations yielded only 85 cases with values at or above this level.

Since the sky surface brightness is conserved by the lensing process, we find the ERO population contributes $1.88 \pm 0.16 \times 10^4$ mJy deg^{-2} to the $850 \mu\text{m}$ EBL. This value is 61 percent of the total $850 \mu\text{m}$ EBL if the Puget et al. (1996) value of 3.1×10^4 mJy deg^{-2} is assumed, or 43 percent if the Fixsen et al. (1998) value of 4.4×10^4 mJy deg^{-2} is assumed. When the galaxies with $3.5 < I - K' < 4$ are included, the contribution increases to $2.59 \pm 0.19 \times 10^4$ mJy deg^{-2} (83 or 59 percent of the total, respectively). Thus, the majority of the $850 \mu\text{m}$ EBL arises from the relatively small number of sources with $I - K' > 3.5$.

However, there may be systematic errors arising from clustering. For the individual fields, the EBL contributions from the $I - K' > 3.5$ sources are $0.81 \pm 0.14 \times 10^4$ mJy deg^{-2} (A370), $6.82 \pm 0.42 \times 10^4$ mJy deg^{-2} (A851), and $3.49 \pm 0.55 \times 10^4$ mJy deg^{-2} (A2390). Although A2390 has the largest number of $I - K' > 3.5$ objects (see § 4), A851 has a higher mean submillimeter signal per object. If we exclude A2390 because of the anomalously high number of red objects in this field, then the $I - K' > 3.5$ population contributes $1.94 \pm 0.15 \times 10^4$ mJy deg^{-2} to the $850 \mu\text{m}$ EBL. While the $I - K' > 3.5$ populations in all three cluster fields are significantly detected, it is clear that a large number of fields would have to be averaged to produce a high precision estimate of the EBL contribution, and the systematic errors in the present estimate may be as high as a factor of 2.

4. THE BREAKDOWN OF THE ERO CONTRIBUTIONS

We now analyze the ERO number counts to determine how representative our fields are and to estimate the ERO surface densities to fainter magnitudes than has previously

been possible. The methodology used is described in more detail in Smith et al. (2002), who analyzed 10 cluster fields observed to shallower K limits.

We used the LENSTOOL software package to determine the amplifications of the EROs, assuming they were located at $z = 2$. (The amplification varies only weakly with redshift for any source beyond $z = 1$ that has a modest amplification.) LENSTOOL uses multiple-component mass distributions that describe the extended potential wells of the clusters and their more massive individual member galaxies (Kneib et al. 1996). Details for the A370, A851, and A2390 clusters can be found in Kneib et al. (1993), Seitz et al. (1996), and J.-P. Kneib et al., in preparation, respectively.

We also used LENSTOOL to determine the areas in the source plane over which an object with a given source plane magnitude would be seen. We created grids the size of our cluster field K' images with $1'' \times 1''$ grid elements and treated the grid points as objects in the source plane at $z = 2$. We brought the grids through the cluster mass distributions to determine the magnifications at each point. Since each point represents one square arcsecond, the associated source plane area for a given magnitude is the sum of the points where an object of that magnitude could be detected.

To compute the ERO surface densities, we summed the reciprocals of the associated areas for all the sources in each magnitude bin. (Multiply imaged sources are correctly handled since the source plane area is proportionally increased relative to the number of images.) The results are shown in Fig. 3, where surface density per square degree per magnitude is plotted versus lensing-corrected (i.e., source plane) isophotal K' magnitude. The fact that Fig. 3 flattens at faint magnitudes indicates that by $K' = 24$ we have already seen most of the K' light density in the ERO population.

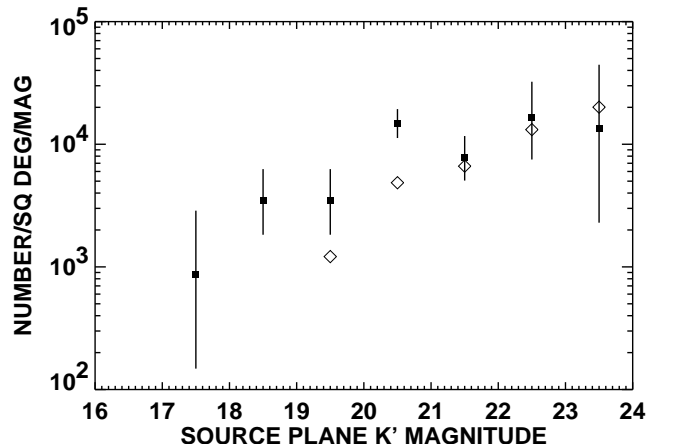


FIG. 3.— Surface density per square degree per magnitude versus lensing-corrected isophotal K' magnitude for the combined K' samples in the A370, A851, and A2390 fields with $I - K' > 4$ (filled squares). The uncertainties are 1σ , based on a Poissonian distribution. The open diamonds show the surface densities when the A2390 field is excluded.

At brighter K' magnitudes our surface densities are higher than those determined by Smith et al. (2002) and by previous blank field surveys (e.g., Barger et al. 1999; Daddi et al. 2000). To $K' = 21.6$ we find a cumulative sur-

face density of 8.0 (6.6, 9.4) EROs per square arcminute, where the parentheses show the 1σ limits. This is slightly more than three times the Smith et al. value of 2.5 ± 0.4 arcmin $^{-2}$. (Our $I - K' = 4$ criterion is very similar to their $R - K > 5.3$ criterion.) The reason for the excess lies in the large population of EROs in the A2390 field, where the surface density is 19.7 (15.6, 23.8) arcmin $^{-2}$ to $K' = 21.6$. If we restrict our analysis to the A370 and A851 cluster fields (the open diamonds in Fig. 3), the surface density drops to 3.4 (2.3, 4.8) arcmin $^{-2}$ to $K' = 21.6$, which is comparable to the Smith et al. value.

Inspection of the K' image of A2390 suggests that the ERO excess in this field corresponds to a cluster of galaxies centered on a bright red galaxy in the northwest corner of the image; this galaxy is an X-ray point source (Fabian et al. 2000) with a spectroscopic redshift of $z = 1.467$ (Cowie et al. 2001). A second X-ray source in the southwest corner has a similar probable spectroscopic redshift (Cowie et al.). If we assume that the excess of EROs is associated with this cluster, then the cluster contains roughly 20 EROs to $K' = 21.6$, making it an extremely large concentration of evolved galaxies at this redshift.

The error-weighted mean 850 μ m flux per source decreases (though slower than linearly) with increasing source plane K' magnitude: at mean K' magnitudes of (16.9, 18.8, 20.6, 22.4) we find error-weighted mean 850 μ m fluxes of (5.18 ± 0.38 , 1.55 ± 0.29 , 1.22 ± 0.14 , 0.47 ± 0.20) mJy. Although submillimeter flux depends only weakly on redshift, such that higher redshift sources fade in K' but not in 850 μ m flux, sources that are fainter in K' luminosity may be intrinsically fainter in 850 μ m luminosity. The dependence of 850 μ m flux on ERO K' magnitude means that brighter submillimeter surveys are more likely to identify ERO counterparts.

The observed decrease in 850 μ m flux with increasing K' magnitude, combined with the flatness of the ERO counts at the fainter magnitudes seen in Fig. 3, implies that the largest contribution to the 850 μ m EBL arises near the point at which the ERO number counts begin to flatten—around $K' = 20$. In the present data half of the 850 μ m light arises in sources with source plane magnitudes $K' < 20$, and half arises in fainter sources, placing the median 850 μ m source at $K' = 20$. If A2390, with its larger number of bright EROs, is excluded, the split occurs at $K' = 20.3$. When sources fainter than $K' = 24$ are included, the split will occur at a fainter magnitude, but the effect will be small.

We may also try to determine if the spectral energy distributions (SEDs) of the sources correlate with the 850 μ m fluxes. If the 850 μ m signal arises primarily from dust-reddened starbursts rather than from old elliptical galaxies, then we would expect objects with a smoother NIR SED to be the primary source of the signal. (The red $I - K'$ colors of old evolved galaxies are in large part due to the 4000 \AA break, which produces a discontinuity in the NIR SEDs.) As illustrated in Fig. 4, we have used the criterion $I - J = 1.8(J - K') - 1.2$ to separate redder $I - J$ galaxies that follow the unevolved elliptical galaxy track from bluer $I - J$ galaxies that lie in the dust-reddened starburst region (see Pozzetti & Mannucci 2000 for other color selection criteria). Sources in the starburst region could also be more recently formed galaxies or galaxies with some residual star formation.

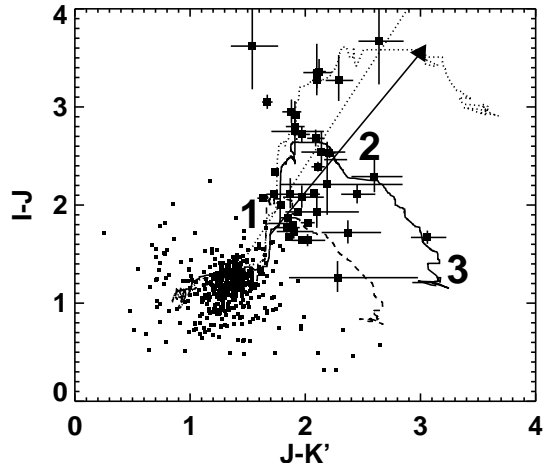


FIG. 4.— $I - J$ versus $J - K'$ for the combined K' samples in the A370, A851, and A2390 fields with measured J magnitudes. Sources with $I - K' > 3.5$ ($I - K' < 3.5$) are denoted by large (small) solid squares; 1σ uncertainties are given for the $I - K' > 3.5$ sources. The dashed, solid, and dotted curves show, respectively, the tracks for an unevolved Sb, Sa, and elliptical galaxy versus redshift from $z = 0$ to $z = 3$. Redshifts $z = 1, 2$, and 3 are marked and labeled on the Sa track. The arrow shows the direction that reddening would move a galaxy using a simple model where extinction is inversely proportional to wavelength. The length of the arrow corresponds to $A_V = 10$. The dotted line $I - J = 1.8(J - K') - 1.2$ roughly separates objects that follow the unevolved elliptical galaxy track (left of the dotted line) from objects located where reddening could move a starburst galaxy (right of the dotted line).

Of the 55 galaxies with $I - K' > 3.5$ in our sample, 39 have measured J magnitudes. The error-weighted mean 850 μ m flux for all 39 objects is 0.90 ± 0.12 mJy. The 17 (44 percent) that satisfy the elliptical galaxy criterion have 0.32 ± 0.18 mJy. In contrast, the 22 that lie on the dusty starburst side have 1.38 ± 0.16 mJy. Thus, the bulk of the signal does appear to arise in the smaller number of galaxies that could be dusty starbursts.

5. SUMMARY

From an optical, NIR, and submillimeter survey of three massive lensing cluster fields we find that VROs and EROs mark, on average, strong submillimeter emitters. The $I - K' > 3.5$ population contributes $1.94 \pm 0.15 \times 10^4$ mJy deg $^{-2}$ to the 850 μ m EBL if we exclude the A2390 field because of the anomalously high number of red objects, and $2.59 \pm 0.19 \times 10^4$ mJy deg $^{-2}$ if we include the A2390 field. These contributions are, respectively, 44–62 percent and 59–83 percent of the 850 μ m EBL (the ranges depend on the measurement of the EBL assumed) and are much larger than the 12–16 percent from galaxies containing bright AGN (Barger et al. 2001). ERO clustering is an important effect that must be accounted for if we are to obtain a better estimate. The median magnitude of the sources giving rise to the EBL is $K' = 20$ to $K' = 20.3$, depending on the cluster sample used. The 850 μ m EBL contribution primarily arises in the subset of the population corresponding to dusty starbursts.

We thank an anonymous referee for helpful comments. AJB gratefully acknowledges support from NSF grant AST-0084847 and from the University of Wisconsin Re-

search Committee with funds granted by the Wisconsin Alumni Research Foundation.

REFERENCES

- Barger, A. J., Cowie, L. L., Trentham, N., Fulton, E., Hu, E. M., Songaila, A., & Hall, D. 1999, *AJ*, 117, 102
- Barger, A. J., Cowie, L. L., & Richards, E. A. 2000, 119, 2092
- Barger, A. J., Cowie, L. L., Steffen, A. T., Hornschemeier, A. E., Brandt, W. N., & Garmire, G. P. 2001, *ApJ*, 560, L23
- Cimatti, A., Andreani, P., Röttgering, H., & Tilanus, R. 1998, *Nature*, 392, 895
- Cimatti, A., et al. 2002, *A&A*, 381, L68
- Cowie, L. L., Gardner, J. P., Lilly, S. J., & McLean, I. 1990, *ApJ*, 360, 1
- Cowie, L. L., et al. 2001, *ApJ*, 551, L9
- Cowie, L. L., Barger, A. J., & Kneib, J.-P. 2002, *AJ*, 123, 2197
- Daddi, E., Cimatti, A., Pozzetti, L., Hoekstra, H., Röttgering, H. J. A., Renzini, A., Zamorani, G., & Mannucci, F. 2000, *A&A*, 361, 535
- Dunlop, J., Peacock, J., Spinrad, H., Dey, A., Jimenez, R., Stern, D., & Windhorst, R. 1996, *Nature*, 381, 581
- Epps, H. W. & Miller, J. S. 1998, *Proc. SPIE*, 3355, 48
- Fabian, A. C., et al. 2000, *MNRAS*, 315, L8
- Fixsen, D. J., Dwek, E., Mather, J. C., Bennet, C. L., & Schafer, R. A. 1998, *ApJ*, 508, 123
- Graham, J. R. & Dey, A. 1996, 471, 720
- Holland, W. S., et al. 1999, *MNRAS*, 303, 659
- Hu, E. M. & Ridgway, S. E. 1994, *AJ*, 107, 1303
- Iverson, R. J., et al. 2002, *MNRAS*, in press (astro-ph/0206432)
- Kneib, J.-P., Mellier, Y., Fort, B., & Mathez, G. 1993, *A&A*, 273, 367
- Kneib, J.-P., Ellis, R. S., Smail, I., Couch, W. J., & Sharples, R. M. 1996, *ApJ*, 471, 643
- Kodama, T., Arimoto, N., Barger, A. J., & Aragón-Salamanca, A. 1998, *A&A*, 334, 99
- Motohara, K., et al. 1998, *Proc. SPIE* 3354, 659
- Oke, J.B., et al. 1995, *PASP*, 107, 375
- Peacock, J. A., et al. 2000, 318, 535
- Pozzetti, L. & Mannucci, F. 2000, *MNRAS*, 317, L17
- Puget, J.-L., Abergel, A., Bernard, J.-P., Boulanger, F., Burton, W. B., Desert, F. -X., & Hartmann, D. 1996, *A&A*, 308, 5
- Seitz, C., Kneib, J.-P., Schneider, P., & Seitz, S. 1996, *A&A*, 314, 707
- Smail, I., Ivison, R. J., Kneib, J.-P., Cowie, L. L., Blain, A. W., Barger, A. J., Owen, F. N., & Morrison, G. 1999, *MNRAS*, 308, 1061
- Smail, I., Ivison, R. J., Blain, A. W., & Kneib, J.-P. 2002, *MNRAS*, 331, 495
- Smith, G. P., Treu, T., Ellis, R., Kneib, J.-P., & Frye, B. L. 2001, *ApJ*, 562, 635
- Smith, G. P., et al. 2002, *MNRAS*, 330, 1
- Soifer, B. T., Matthews, K., Neugebauer, G., Armus, L., Cohen, J. G., Persson, S. E., & Smail, I. 1999, *AJ*, 118, 2065
- Spinrad, H., Dey, A., Stern, D., Dunlop, J., Peacock, J., Jimenez, R., & Windhorst, R. 1997, *ApJ*, 484, 581